Bulletin of the Seismological Society of America. Vol. 61, No. 6, pp. 1755–1770. December, 1971

SURFACE MOTION OF A SEMI-CYLINDRICAL ALLUVIAL VALLEY FOR INCIDENT PLANE *SH* WAVES

By M. D. Trifunac

ABSTRACT

The nature of surface motion in and around a semi-cylindrical alluvial valley is investigated for the case of incident plane *SH* waves. The closed-form analytical solution of this two-dimensional wave-propagation problem displays complicated wave-interference phenomena characterized by nearly-standing wave patterns, rapid changes in the ground-motion amplification along the free surface of the valley, and significant dependence of motion on the incidence angle of *SH* waves. Although simple, this model may qualitatively explain some vibrating characteristics of long and deep alluvial valleys.

Introduction

One of the major concerns of engineering seismology is to understand and explain vibrational properties of the soil excited by near earthquakes. Alluvial deposits, often very irregular geometrically, may affect significantly the amplitudes of incident seismic waves. Since many human settlements are founded on alluvial valleys, it is important for the design of earthquake resistant structures to study the mechanism of these amplification effects. The main purpose of this paper will be, therefore, to point out some phenomena associated with the two-dimensional-wave interference.

Many observed properties of the ground amplification of seismic waves have been explained by a simple model of alluvial deposits consisting of horizontally stratified surface layers overlying a half-space (e.g., Tsai 1969). Other equally important characteristics of strong earthquake ground motion caused by irregular layer properties (e.g., Aki and Larner 1970; Boore 1970), focusing of seismic waves, and standing waves call for other geometrically more complex models.

In this paper, we investigate the amplification and focusing properties of the semi-cylindrical alluvial valley subjected to incident *SH*-waves. This relatively simple model allows a closed-form analytical solution, but, at the same time, leads to complicated interference phenomena that probably also take place in realistic alluvial valleys.

There are only a few known geological configurations with a cross-section resembling the semi-cylindrical valley and whose length is sufficiently great to permit the two-dimensional analysis. Two such examples might be the Barnard Glacier in the St. Elias Mountain Range, Alaska, and the floor of the Yosemite Valley, California (Gutenberg *et al.* 1956). (I am indebted to Professor R. P. Sharp of the California Institute of Technology for bringing these examples to my attention.)

The Model

The two-dimensional model to be analyzed is shown in Figure 1. It consists of a semi-cylindrical valley of radius a. The soil is assumed to be elastic, isotropic and homogeneous, and the contact between the valley and the half-space is assumed to be welded. The material properties are given by the rigidity μ and the velocity of the shear waves β. The subscript v on μ and β designates these constants in the valley.

Excitation. We assume that the half-space is subjected to the incident motion

$$u_z^{\,i} = e^{i\omega[t-(x/c_x)+(y/c_y)]} \tag{1}$$

which represents a plane *SH* wave traveling upward and to the right (Figure 1) along a ray which makes an angle γ with the y axis. The phase velocities along the x axis c_x and the y axis c_y are given by

$$c_x = \beta/\sin\gamma \tag{2}$$

$$c_y = \beta/\cos\gamma. \tag{3}$$

The motion represented by u_z is in the z direction only and is the same for all z.

Far from the valley u_z^i waves are reflected from the free surface and incident u_z^i and reflected u_z^r waves interfere to give the resulting free-field motion

$$u_z^i + u_z^r = 2e^{i\omega[t-(x/c_x)]} \cos\left(\frac{\omega y}{c_y}\right). \tag{4}$$

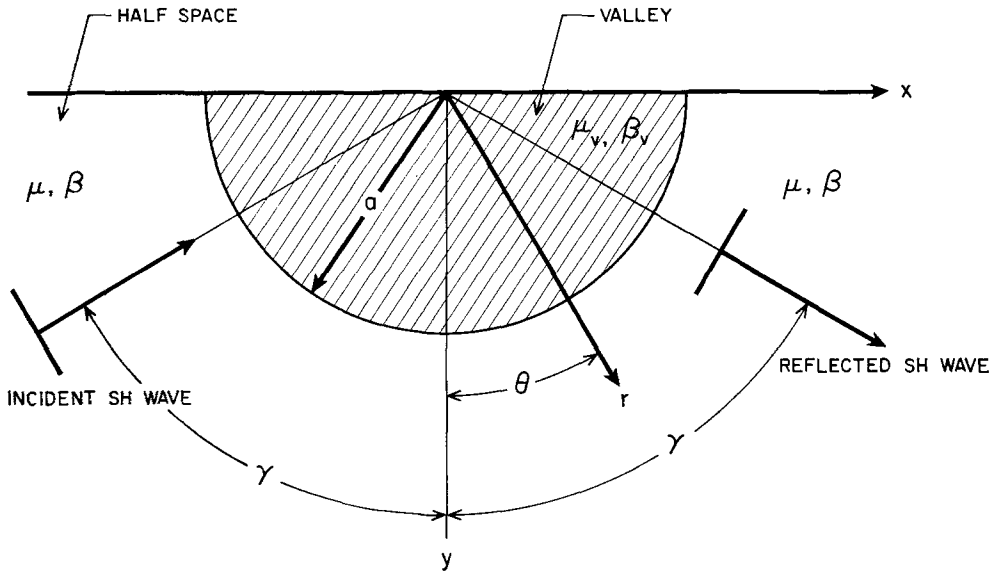

FIG. 1. Semi-cylindrical valley and the surrounding half-space.

Close to the valley, the total motion is given by (4) and also the waves reflected and diffracted by the material discontinuity at $r = a$ (Figure 1). We call these additional waves u_z^R.

The geometry of the valley (Figure 1) is suitable for the use of a cylindrical coordinate system; therefore, it is convenient to represent (4) in terms of functions that depend on cylindrical coordinates r and θ. It can be shown, then, that (4) becomes (Watson, 1966)

$$u_z^i + u_z^r = 2J_0(\kappa r) + 4\sum_{n=1}^{\infty}(-1)^n J_{2n}(\kappa r)\cos 2n\gamma \cos 2n\theta$$

$$- 4i\sum_{n=0}^{\infty}(-1)^n J_{2n+1}(\kappa r)\sin(2n+1)\gamma \sin(2n+1)\theta. \tag{5}$$

Here $J_p(x)$ are the Bessel functions of the first kind with argument x and order p and $\kappa = \omega/\beta$.

Solution of the problem. The total displacement u_z in the half-space and ${}_vu_z$ in the valley must satisfy the differential equation

$$\frac{\partial^2 u}{\partial r^2} + \frac{1}{r}\frac{\partial u}{\partial r} + \frac{1}{r^2}\frac{\partial^2 u}{\partial \theta^2} = \frac{1}{\beta^2}\frac{\partial^2 u}{\partial t^2} \tag{6}$$

where u stands for either u_z or ${}_vu_z$.

The boundary conditions are

$$\sigma_{\theta z} = \frac{\mu}{r}\frac{\partial u_z}{\partial \theta} = 0 \quad \text{at} \quad \theta = \pm\frac{\pi}{2} \tag{7}$$

$$u_z = {}_vu_z \quad \text{at} \quad r = a \tag{8}$$

and

$$\mu\frac{\partial u_z}{\partial r} = \mu_v\frac{\partial_v u_z}{\partial r} \quad \text{at} \quad r = a. \tag{9}$$

The total motion in the half-space can be expressed as the superposition of $(u_z{}^i + u_z{}^r)$ and the waves $u_z{}^R$ reflected and diffracted by the discontinuity at $r = a$. The $u_z{}^R$ must represent a wave outgoing from the valley. This wave has to satisfy the differential equation (6) and the boundary conditions (7), (8), and (9). We write $u_z{}^R$ as

$$u_z{}^R = \sum_{n=0}^{\infty} [a_n H_{2n}^{(2)}(\kappa r)\cos 2n\theta + b_n H_{2n+1}^{(2)}(\kappa r)\sin(2n+1)\theta \tag{10}$$

where

$$\kappa = \frac{\omega}{\beta}. \tag{11}$$

The $H_p^{(2)}(x)$ is the Hankel function of the second kind with argument x and order p. In addition to satisfying (6), (7), (8), and (9) the motion in the valley must have finite amplitudes at $r = 0$. It may be written as

$${}_vu_z = c_0 J_0(\kappa_v r) + \sum_{n=1}^{\infty} c_n J_{2n}(\kappa_v r)\cos 2n\theta + \sum_{n=0}^{\infty} d_n J_{2n+1}(\kappa_v r)\sin(2n+1)\theta \tag{12}$$

where

$$\kappa_v = \frac{\omega}{\beta_v}. \tag{13}$$

It is readily seen that the waves (5), (10), and (12) satisfy differential equation (6) and the boundary condition (7).

The complex constants a_n, b_n, c_n, and d_n for $n = 0, 1, 2, \cdots$ may next be determined by putting (5), (10), and (12) in the boundary conditions (8) and (9). The result is:

for $n = 0$

$$\begin{aligned} c_0 J_0(\kappa_v a) - a_0 H_0^{(2)}(\kappa a) &= 2J_0(\kappa a) \\ c_0\kappa_v\mu_v a J_1(\kappa_v a) - a_0\kappa\mu a H_1^{(2)}(\kappa a) &= 2\kappa\mu a J_1(\kappa a) \end{aligned} \tag{14a}$$

for $n = 1, 2, \cdots$

$$c_n J_{2n}(\kappa_v a) - a_n H^{(2)}_{2n}(\kappa a) = 4(-1)^n J_{2n}(\kappa a) \cos 2n\gamma$$

$$c_n \mu_v [\kappa_v a J_{2n-1}(\kappa_v a) - 2n J_{2n}(\kappa_v a)] - a_n \mu [\kappa a H^{(2)}_{2n-1}(\kappa a) - 2n H^{(2)}_{2n}(\kappa a)]$$
$$= 4(-1)^n \mu [\kappa a J_{2n-1}(\kappa a) - 2n J_{2n}(\kappa a)] \cos 2n\gamma \quad (14b)$$

and for $n = 0, 1, 2, \cdots$

$$d_n J_{2n+1}(\kappa_v a) - b_n H^{(2)}_{2n+1}(ka) = -4i(-1)^n J_{2n+1}(\kappa a) \sin (2n+1)\gamma$$

$$d_n \mu_v [\kappa_v a J_{2n}(\kappa_v a) - (2n+1) J_{2n+1}(\kappa_v a)] - b_n \mu [\kappa a H^{(2)}_{2n}(\kappa a) - (2n+1) H^{(2)}_{2n+1}(\kappa a)]$$
$$= -4i(-1)^n \mu [\kappa a J_{2n}(\kappa a) - (2n+1) J_{2n+1}(\kappa a)] \sin (2n+1)\gamma. \quad (15)$$

The constants c_n and a_n are given by the equations (14) while d_n and b_n are given by the equations (15). The motion in the valley, for $r \leqq a$ is then given by (12) and, for $r \geqq a$, it becomes

$$u_z = u_z^{\,i} + u_z^{\,r} + u_z^{\,R} \quad (16)$$

where $u_z^{\,i} + u_z^{\,r}$ is given by (5) and $u_z^{\,R}$ by (10).

Surface Displacement Spectra

A question of primary interest for the earthquake engineering studies is the spatial and frequency dependence of the strong earthquake ground motion. For the model studied in the paper, we assumed the excitation to be a steady train of propagating *SH* waves whose incidence angle is γ, the amplitude is 1, and the frequency is ω. The solutions u_z given by (16), and ${}_v u_z$ given by (12), now give spectral amplitudes, since the amplitude of the incident wave (1) is taken to be unity.

Both u_z and ${}_v u_z$ are complex. The amplitudes and phases of these quantities are given as follows

$$|u| \equiv [(\mathrm{Re}\, u)^2 + (\mathrm{Im}\, u)^2]^{1/2} \quad (17)$$

$$\varphi \equiv \tan^{-1}\left[\frac{\mathrm{Im}\, u}{\mathrm{Re}\, u}\right]. \quad (18)$$

Both $|u|$ and φ depend on the frequency of the incident waves, the radius of the semi-cylindrical valley, material constants ρ, ρ_v, ($\rho = \mu/\beta^2$; $\rho_v = \mu_v/\beta_v^{\,2}$), β and β_v and coordinates r and θ, or in terms of dimensionless quantities, on κa, ρ/ρ_v, β/β_v, r/a and θ. The parameter κa given by

$$\kappa a = \frac{\omega a}{\beta} \quad (19)$$

can also be expressed as

$$\kappa a = \frac{2\pi a}{\lambda} \quad (20)$$

where $\lambda = \beta T$ is the wavelength of the incident wave. It is then convenient to think in terms of a ratio η given by

$$\eta = \frac{2a}{\lambda}. \tag{21}$$

Then κa is given by $\pi\eta$.

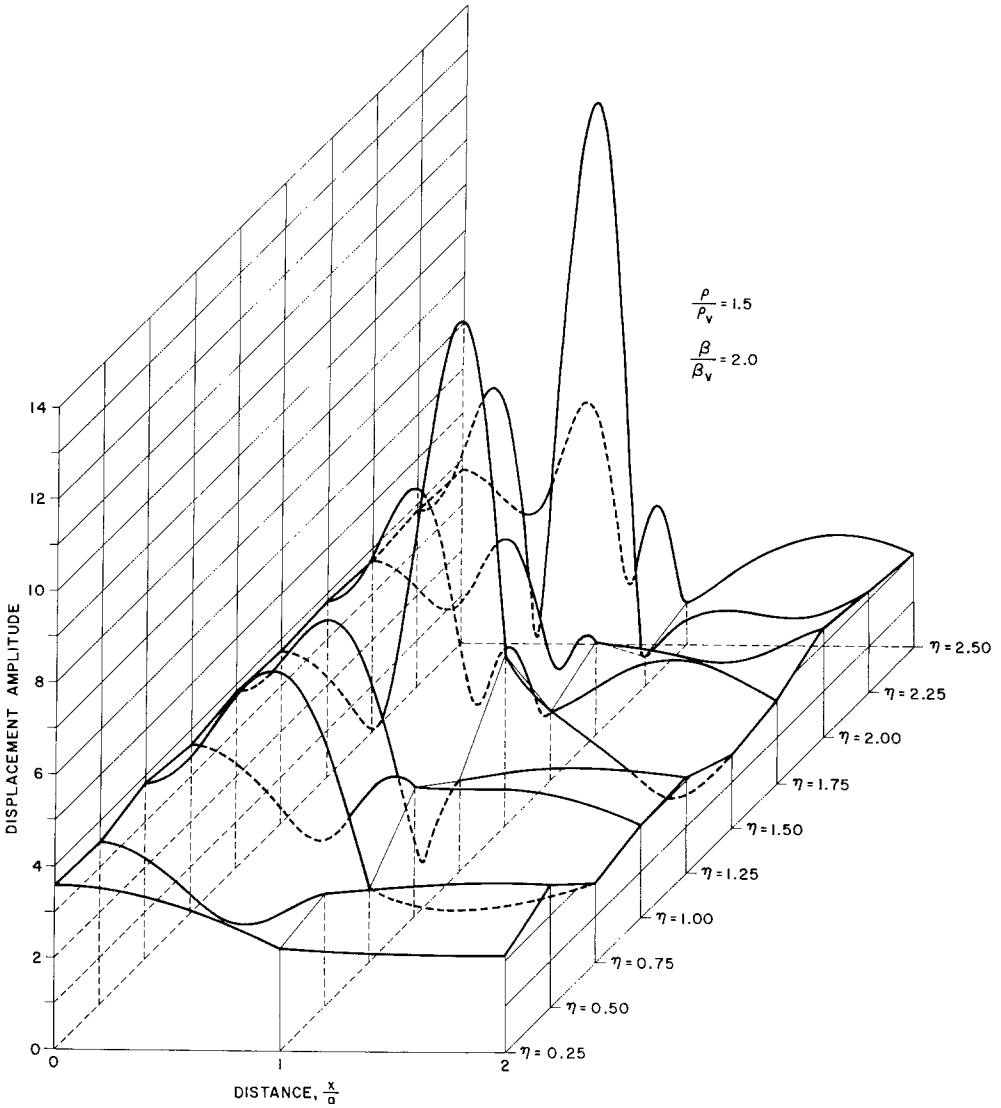

FIG. 2. Envelope of surface displacements for vertical incidence ($\gamma = 0°$) of *SH* waves plotted versus the dimensionless frequency η.

Figures 2, 3 and 4 give the envelope of surface displacements for $\eta = 0.25, \cdots, 2.50$, for different values of ρ/ρ_v and β/β_v, and for the vertical incidence ($\gamma = 0°$) of *SH* waves whose amplitude is one. The surface displacement amplitudes that correspond to the amplification factors are plotted on the vertical axis. The two horizontal axes in Figures 2, 3, and 4 are x/a and η. The point $x/a = 1$ corresponds to the edge of the valley, and $x/a = 0$, to the center of the valley. Since all motions are symmetric about $x/a = 0$, for vertical incidence of *SH* waves, only the positive x/a axis is illustrated.

In Figures 2 and 3 both ρ/ρ_v and β/β_v are greater than one. This corresponds to a "softer" material in the valley and "harder" material outside the valley. Figure 4, for which $\rho/\rho_v = 0.666$ and $\beta/\beta_v = 0.5$, is an example of "harder" material in the valley and "softer" material outside. As may been seen from those figures, surface-displacement amplitudes for $\rho/\rho_v > 1$ and $\beta/\beta_v > 1$ are complicated in the "soft" valley by the interference phenomena caused by the semi-cylindrical interface $r = a$. Displacement amplitudes outside the valley ($x/a \geqq 1$) are less complicated, and although they are

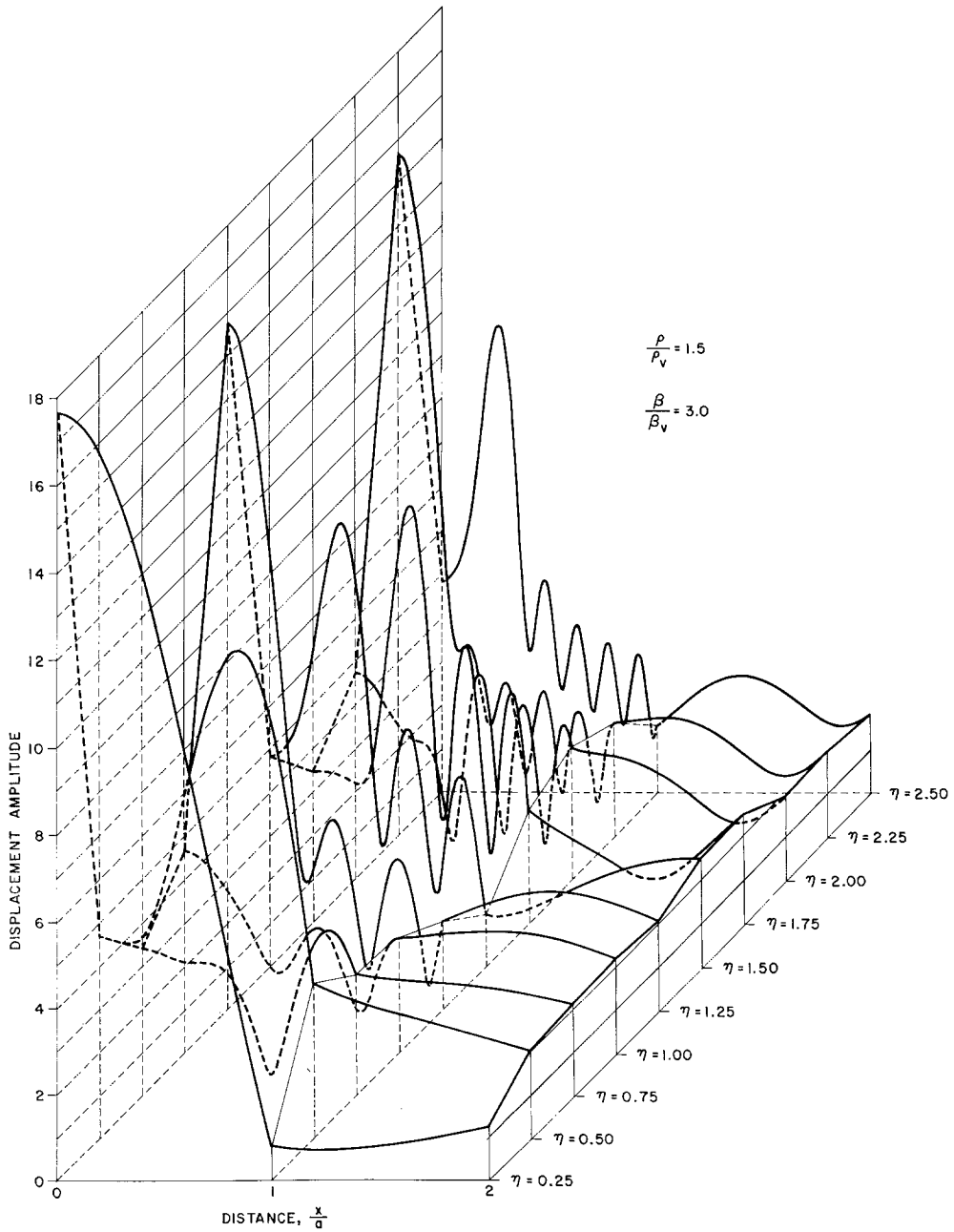

FIG. 3. Envelope of surface displacements of vertical incidence ($\gamma = 0°$) of *SH* waves plotted versus the dimensionless frequency η.

shown only for $1 \leqq x/a \leqq 2$ it can be seen that for increasing x/a, displacement amplitudes tend to the amplification value of 2. This is as expected, because the "free field" surface-displacement amplitude, far from the valley, corresponding only to $u_z^i + u_z^r$, is 2.

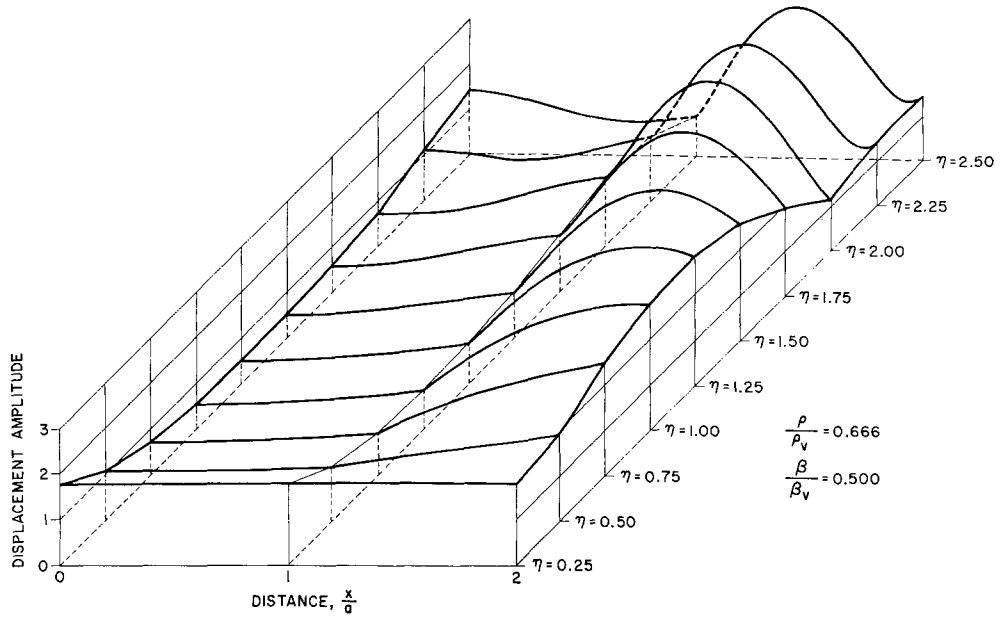

FIG. 4. Envelope of surface displacements for vertical incidence ($\gamma = 0°$) of *SH* waves plotted versus the dimensionless frequency η.

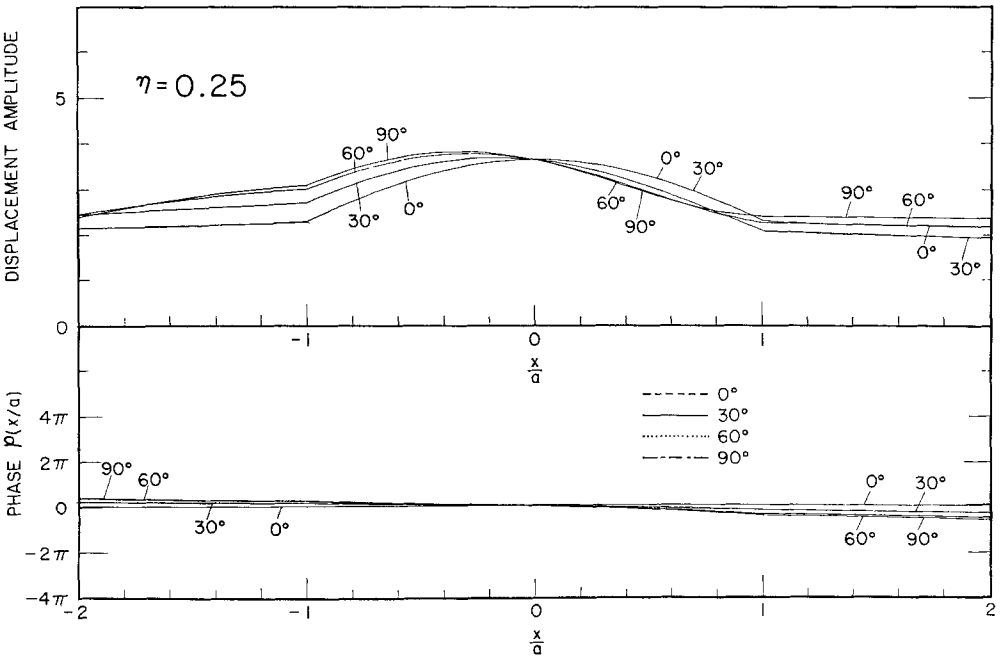

FIG. 5. Surface-displacement amplitudes and phases for incident ($\gamma = 0°$, 30°, 60°, and 90°) plane *SH* waves. $x/a = 0$ corresponds to the center of the semi-cylindrical valley and $x/a = \pm 1$ to the edges of the valley.

It may be of interest to compare results in Figures 2, 3 and 4 with those for a single surface layer of constant thickness $H = a$ subjected to the vertically-incident plane SH waves. By using the same notation for the material properties μ_v and β_v in the surface layer, as in the case of the semi-cylindrical valley, it can be shown (e.g., Haskell 1960) that the surface-displacement amplification of vertically-incident waves caused by a layer of thickness H is given by

$$\text{amplification} = \frac{1}{\left[\cos^2 \frac{\omega H}{\beta_v} + \left(\frac{\mu_v}{\mu}\frac{\beta}{\beta_v}\right)^2 \sin^2 \frac{\omega H}{\beta_v}\right]^{1/2}}. \tag{22}$$

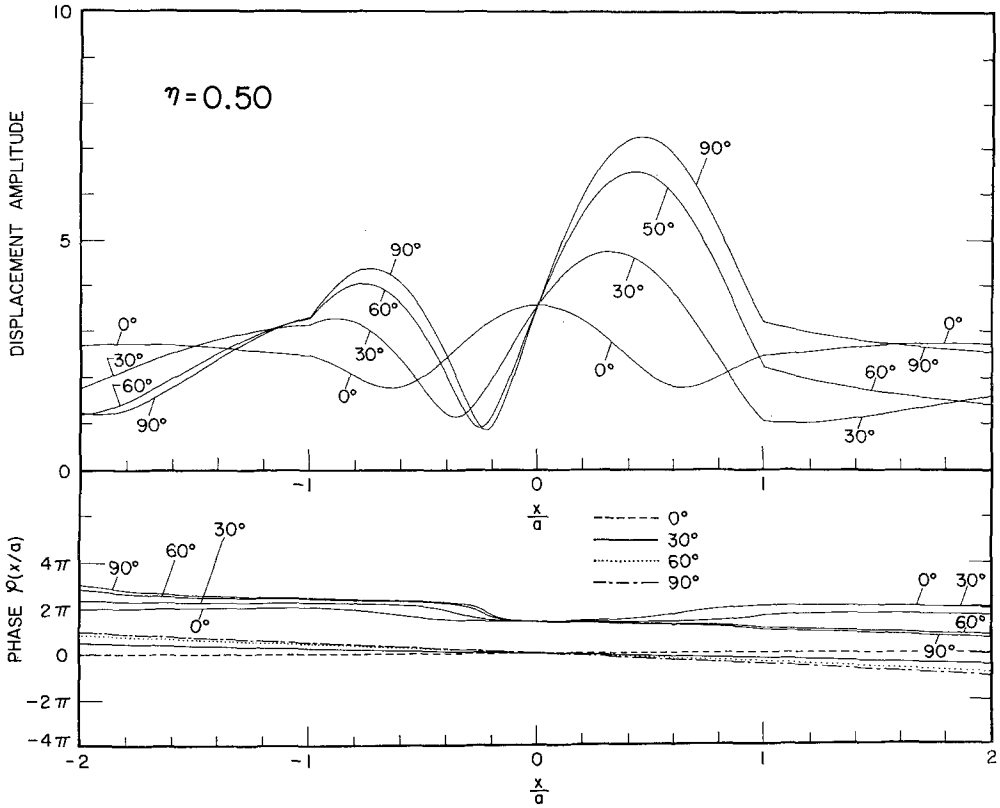

FIG. 6. Surface-displacement amplitudes and phases for incident (γ = 0°, 30°, 60°, and 90°) plane SH waves. $x/a = 0$ corresponds to the center of the semi-cylindrical valley and $x/a = \pm 1$ to the edges of the valley.

The maxima of this function are attained for

$$\frac{\omega H}{\beta_v} = \left(n + \frac{1}{2}\right)\frac{\pi}{2} \tag{23}$$

and are equal to

$$\text{amplification max.} = \frac{\mu\beta_v}{\mu_v\beta}.$$

Taking $\lambda_v = T\beta_v$ and $\lambda = T\beta$ and defining $\eta = 2H/\lambda$, (23) gives

$$\eta = \frac{\beta_v}{\beta}\left(\frac{n}{2} + \frac{1}{4}\right); \qquad n = 0, 1, 2, \cdots. \tag{24}$$

For example, for $\beta_v/\beta = \frac{1}{3}$ in Figure 3, the model with a layer of uniform thickness $H = a$ would predict maxima of the ground-displacement amplitudes in the center of the semi-cylindrical valley to be at $\eta = \frac{1}{12}, \frac{3}{12}, \frac{5}{12}, \cdots$. For example, from Figure 3, we find that $\eta = \frac{3}{12}$ and $\frac{15}{12}$ indeed give high amplifications, whereas $\eta = \frac{9}{12}$ and $\frac{21}{12}$, which according to (24) would also be expected to give maxima, yield only very small amplitudes. The model with a layer of constant thickness $H = a$ would also predict the amplification to be 9 for the center of the semi-cylindrical valley in Figure 3. The amplification for the semi-cylindrical valley is apparently almost twice that much.

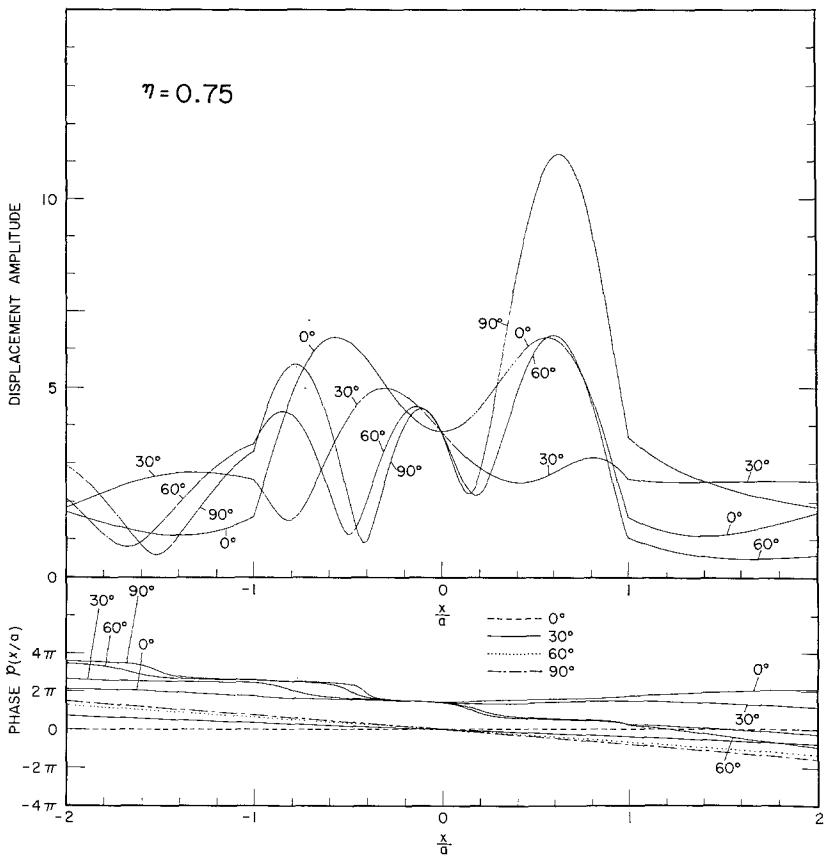

FIG. 7. Surface-displacement amplitudes and phases for incident (γ = 0°, 30°, 60°, and 90°) plane *SH* waves. $x/a = 0$ corresponds to the center of the semi-cylindrical valley and $x/a = \pm 1$ to the edges of the valley.

The above qualitative comparison shows that when the interface of the alluvial valley becomes steep and the depth of the valley becomes comparable to its width, the simple model with a layer of uniform thickness $H = a$ does not apply. When the interface slopes are small, i.e., when the width to the depth ratio is large, the above-mentioned simple model may give reasonable estimates of the surface-displacement amplification (Aki and Larner 1970).

Dependence of Displacement Spectra on Incidence Angle γ

The amplification spectra of Figures 2, 3 and 4 were given for the vertical incidence of plane *SH* waves ($\gamma = 0°$). In this section, we investigate how these spectra change for different angles γ. Figures 5 to 10 give surface-displacement amplification versus di-

mensionless distance x/a plotted for $\eta = 0.25, 0.50, 0.75, 1.00, 1.25$ and 1.50. In these figures, $x/a = 0$ corresponds to the center of the semi-cylindrical valley, and $x/a = \pm 1$, to the edges of the valley. In each figure, the displacement amplification and its phase $\varphi(x/a)$ are plotted for the incidence angles $\gamma = 0°, 30°, 60°$ and $90°$. The phase $\varphi(x/a)$, defined by (18), is plotted relative to the phase $\varphi(0)$ in the center of the valley. For $\rho/\rho_v = 1$ and $\beta/\beta_v = 1$, the solution of the wave equation (6) would reduce to (4) and would be valid for all r. In this case, the phase $\varphi(x/a)$ would be given by

$$\varphi(x/a) = -\frac{\omega x}{c_x} = -\left(\frac{\omega a}{c_x}\right)\frac{x}{a} \tag{25}$$

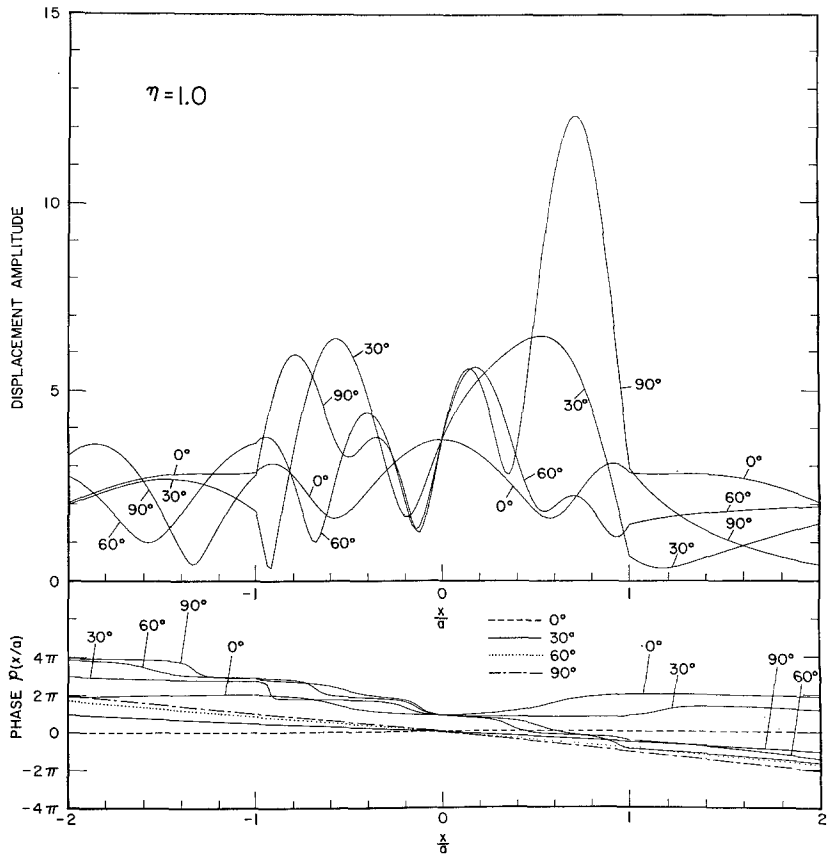

FIG. 8. Surface-displacement amplitudes and phases for incident ($\gamma = 0°, 30°, 60°$, and $90°$) plane SH waves. $x/a = 0$ corresponds to the center of the semi-cylindrical valley and $x/a = \pm 1$ to the edges of the valley.

and by (2), $\omega a/c_x$ becomes

$$\frac{\omega a}{c_x} = \frac{\omega a}{\beta}\sin\gamma. \tag{26}$$

Thus, for $\rho/\rho_v = 1$ and $\beta/\beta_v = 1$, $\varphi(x/a)$ is a straight line with a negative slope given by (26). These straight lines passing through $x/a = 0$ are also plotted in Figures 6 to 10, for comparison with the $\varphi(x/a)$ calculated for a semi-cylindrical valley. For $\eta =$

0.25 these straight lines are omitted, because they fall too close to the computed $\varphi(x/a)$ and would only confuse the phase diagram in Figure 5. All diagrams in Figures 5 to 10 were calculated for $\rho/\rho_v = 1.5$ and $\beta/\beta_v = 2$, a case which corresponds to the spectra in Figure 2.

Several important properties of the model in Figure 1 are reflected in Figures 2 to 10. First, it is clear that as η increases, i.e., as the incident wavelength λ decreases, the effects of the valley on the "free field" motion increase. This result is analogous to the intuitive physical expectation that the waves with long wavelength do not "feel"

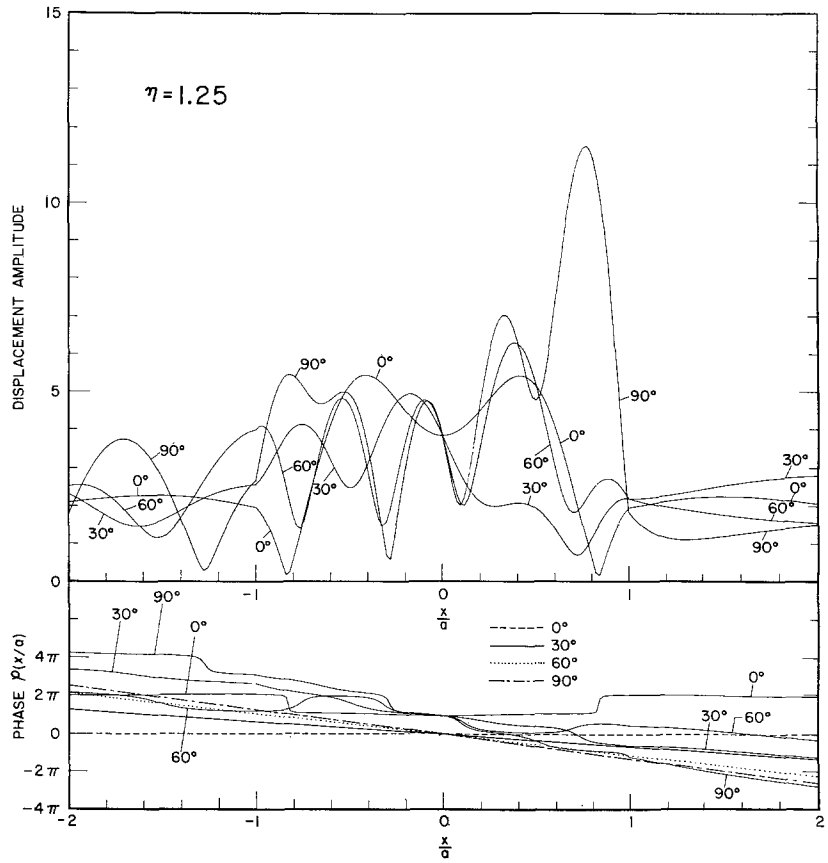

FIG. 9. Surface-displacement amplitudes and phases for incident (γ = 0°, 30°, 60°, and 90°) plane *SH* waves. $x/a = 0$ corresponds to the center of the semi-cylindrical valley and $x/a = \pm 1$ to the edges of the valley.

small irregularities in the ground, whereas the waves with short wavelengths do. Second, Figures 2, 3 and 4 show that for increasing β/β_v, that is, for the "softer" material in the valley, over-all amplification in the valley increases. Again, this result is in agreement with what would be expected. Third, for $\beta/\beta_v > 1$ and $\rho/\rho_v > 1$, there are many sections along the surface of the valley where significantly-high local amplifications take place. These regions are not necessarily confined to the deepest part of the valley and apparently depend on β/β_v and ρ/ρ_v, as can be seen from Figures 2, 3 and 4. For example, for $\beta/\beta_v = 2$ and $\rho/\rho_1 = 1.5$ in Figures 6 to 10, the region of such high amplification is mainly concentrated toward the edges of the valley.

The localized high amplification of the surface displacements is a consequence of the

focusing of waves reflected through the discontinuity at $r = a$. To explain this, it may be convenient to think in terms of many parallel rays incident from the underlying medium. The change in the ray direction upon the refraction at $r = a$ depends only on the ratio β/β_v, and depending on the interference pattern of all rays, some points in the valley and along its surface receive a high concentration of incident rays, which, if they constructively interfere, increase the local displacement amplitude.

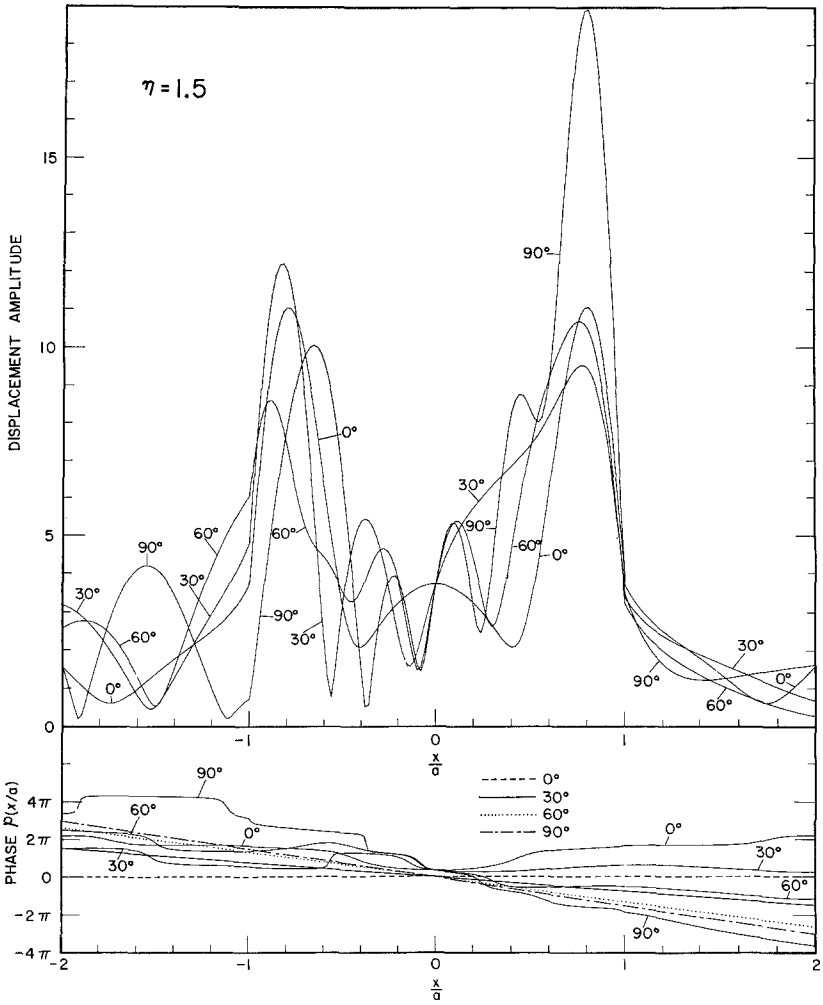

FIG. 10. Surface-displacement amplitudes and phases for incident (γ = 0°, 30°, 60°, and 90°) plane SH waves. $x/a = 0$ corresponds to the center of the semi-cylindrical valley and $x/a = \pm 1$ to the edges of the valley.

Another property of the model in Figure 1 is that, for increasing γ, the pattern of the surface amplification changes so that the motions in the region of positive x/a increase and in the region of negative x/a decrease relative to the symmetric incidence with $\gamma = 0°$. This property again may be interpreted by the ray analogy. For increasing γ, all incident rays (Figure 1) enter the valley from the left, while a shadow zone is formed on the right. The rays refracted into the valley, predominantly from the left interface, are partly or completely reflected from the right interface back into the valley. The

amplification caused by focusing of these waves is apparently greater for positive x/a and for $\rho/\rho_v = 1.5$ and $\beta/\beta_v = 2$.

Finally, as can be seen in Figures 5 to 10, vibrations in some regions in the valley are characterized by nearly-standing waves. These regions correspond to the intervals along x/a in Figures 5 to 10, for which $\varphi(x/a)$ is nearly stationary. Furthermore, there are many points along x/a, particularly for greater η, where rapid change in phase takes place and at the same time displacement amplitudes are zero (e.g., $x/a = \pm 0.85$, in Figure 9, or $x/a = -0.38, -1.90$, in Figure 10). This property of the complicated in-

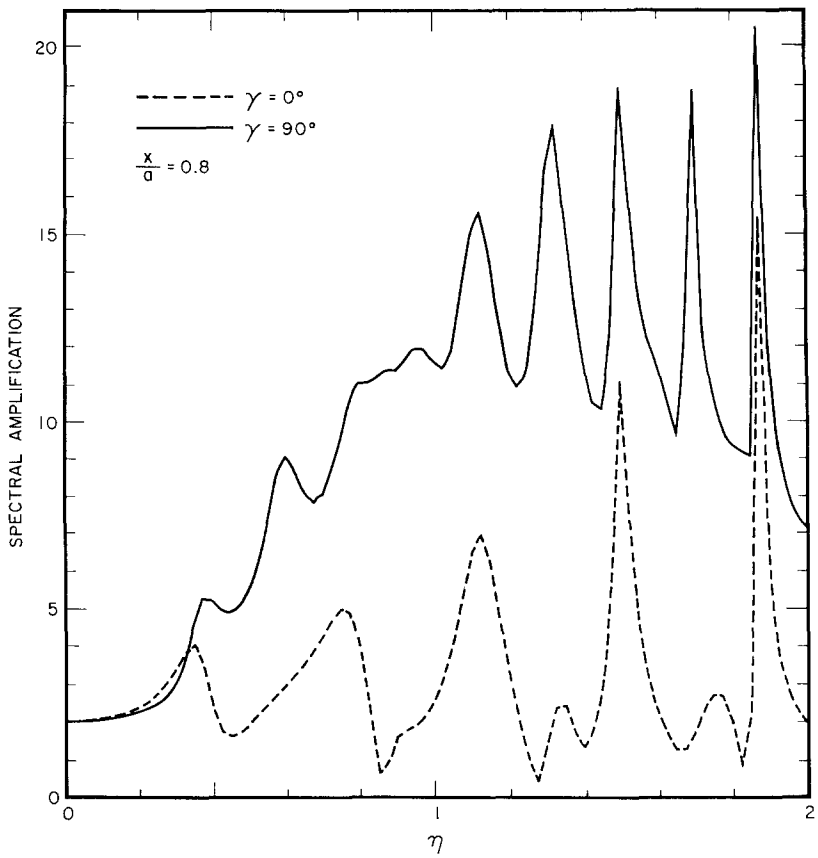

FIG. 11. Typical spectral amplification on the surface of the semi-cylindrical valley at $x/a = 0.8$ ($\rho/\rho_v = 1.5$; $\beta/\beta_v = 2.0$) plotted versus the dimensionless frequency η.

terference pattern in the valley is of interest to earthquake engineering, because it suggests that some structures could be excited predominantly into torsional oscillations.

TYPICAL SPECTRA

The Figures 11 and 12 show the typical spectral amplification on the surface of the semi-cylindrical valley, plotted versus dimensionless frequency η. Figure 11 compares spectra for the vertical and horizontal incidence at x/a, 0.8, while Figure 12 gives the same comparison for $x/a = -0.8$.

Although the spectra in Figures 11 and 12 represent only one typical case for $\rho/\rho_v = 1.5$ and $\beta/\beta_v = 2.0$ and for $x/a = \pm 0.8$, several general properties of the model in Figure 1 are nevertheless well displayed. One of these properties, as already men-

tioned above, is that long-period waves (λ large) do not "feel" small irregularities in the ground. This is shown in Figures 11 and 12 where as η tends to zero, spectral amplification tends to 2, corresponding to the "free field" amplification.

The most important property of the spectra in Figures 11 and 12 is that the amplitude and position of many local peaks depend on x/a and γ. This property of the model in Figure 1 may serve as a warning to all simple interpretations of the recorded strong-motion accelerograms and microtremor ground noise. It clearly shows that unless the direction of the approach of the main disturbance and the detailed geology of the site

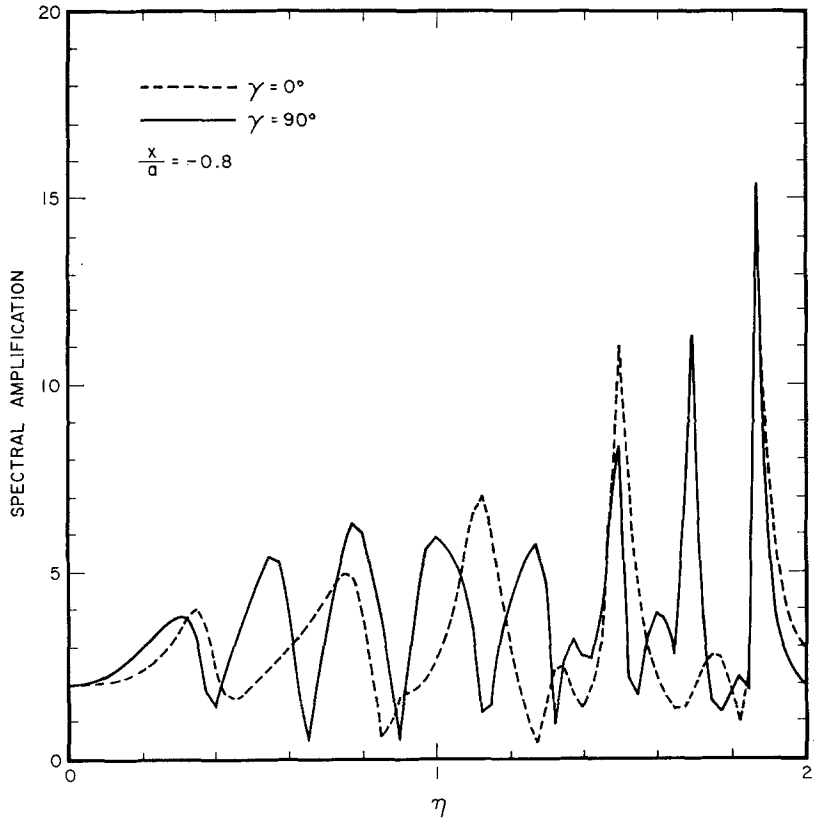

FIG. 12. Typical spectral amplification on the surface of the semi-cylindrical valley at $x/a = -0.8$ ($\rho/\rho_v = 1.5$; $\beta/\beta_v = 2.0$) plotted versus the dimensionless frequency η.

are known, interpretations based on correlating the observed spectral peaks with those from the simple models may be in error.

STANDING WAVES

The model considered in this paper can be used to interpret vibrational characteristics of some simple deep and long alluvial valleys. It points out several phenomena that may take place during strong earthquake ground motion. Among these are the focusing of earthquake waves by the semi-cylindrical material discontinuity and nearly-standing waves generated by the interference in the geometrically-complex alluvium.

A typical observation made during strong earthquake ground motion that might be

related to the phenomenon of standing waves is quoted from Richter (1958): "... seismic waves... travel at speeds measurable in miles per second and cannot possibly be followed by an observer's eye. Waves actually seen would have to be of another physical type with much lower velocities. They might, however, be a modification of standing waves; that is, an interference pattern of nodes and loops may be set up which shifts over the ground as the exciting disturbance changes. A high school instructor described to the author what he saw in the streets at Long Beach in 1933; it could, easily, be such pattern of nodes and loops. There was no suggestion of large motion of the surface of the ground, but the loops or antinodes were put in evidence by dust thrown into the air, while the nodes appeared quiet. The account was rather convincing because the observer was not a physicist and did not have the technical vocabulary used here."

Several accounts on the visible waves are given by Fuller (1912), Lomnitz (1970), and Vitaliano and Vitaliano (1971).

Conclusions

The analysis of the amplification and interference effects on incident plane *SH* waves in a semi-cylindrical valley may qualitatively explain several ground amplification phenomena either observed or recorded during the strong earthquake ground motion and the microtremor noise measurements. From the engineering point of view, the main results of the present analysis that bear on these phenomena may be summarized as follows:

1. The surface-displacement amplification for the semi-cylindrical valley may change rapidly over short distances, in some cases, only a fraction of the characteristic length of the valley. The changes in the amplification over these short distances may be as much as one order of magnitude. For the fixed geometrical and physical properties of the valley and its surrounding medium, the degree of complexity of the amplification pattern increases with the increase of frequency of the incident waves.

2. A comparison of the amplification pattern in the semi-cylindrical valley with the radius $r = a$ and a layer of the uniform thickness $H = a$ shows that there is no simple correspondence in the amplification patterns. The reason for this is related to the one-dimensional nature of the layer model and the two-dimensional nature of the semi-cylindrical valley. This conclusion is important for many engineering applications if the effects of local sites are modeled by horizontal layers of uniform thickness.

3. The pattern of spectral amplification at a given point on the surface of the semi-cylindrical valley significantly depends on the angle of incidence of the *SH* waves. This dependence is reflected in the over-all change of spectrum amplitudes, the shifting of some spectrum peaks from one frequency to another, and in some cases, the complete disappearance or occurrence of peaks as γ varies from 0° to 90°.

4. If the shear-wave velocity in the semi-cylindrical valley decreases, other model properties being fixed, the over-all amplification in the valley increases. For incident *SH* wavelengths longer than 10 to 20 radii of the valley, the amplification in the valley is negligible.

5. In some parts of the valley the interference of *SH* waves may lead to a nearly-standing wave pattern. As a result, at a node, the surface ground motion is zero. Since the phase of the ground motion may change through one π there, a building structure that appears to be centered at such a node might experience essentially pure torsional vibrations and no lateral vibrations at all. This is of course based on the assumption that we are dealing with *SH* waves only.

Acknowledgments

I am indebted to L. Alsop, J. Dorman, B. Isacks, K. Jacob, T. Matumoto and J. Healy of the Lamont-Doherty Geological Observatory and to A. Vijayaraghavan of the California Institute of Technology for critically reading the manuscript and offering many valuable suggestions.

This research was supported in part by the National Science Foundation Grants GA 22709 and GA 29632.

References

Aki, K. and K. Larner (1970). Surface motion of a layered medium having an irregular interface due to incident plane *SH* waves, *J. Geophys. Res.* **75**, 933–954.

Boore, D. (1970). Love waves in nonuniform wave guides: finite difference calculation, *J. Geophys. Res.* **75**, 1512–1527.

Fuller, M. L. (1912). The New Madrid earthquake, *U. S. Geol. Survey Bull.* **494**, p. 115.

Gutenberg, B., J. P. Buwalda, and R. P. Sharp (1956). Seismic explorations on the floor of Yosemite Valley, California, *Bull. Geol. Soc. Am.* **67**, 1051–1078.

Haskell, N. (1960). Crustal reflection of plane *SH* waves, *J. Geophys. Res.* **65**, 4147–4150.

Lomnitz, C. (1970). Some observations of gravity waves in the 1960 Chile earthquake, *Bull. Seism. Soc. Am.* **60**, 660–670.

Richter, C. F. (1958). *Elementary Seismology*, W. H. Freeman and Co., San Francisco.

Tsai, N. C. (1969). *Influence of Local Geology on Earthquake Ground Motion*, Earthquake Engineering Research Laboratory, California Institute of Technology, Pasadena.

Vitaliano, C. T. and D. B. Vitaliano (1971). Gravity waves in the 1954 Fallon, Nevada, earthquake, *Bull. Seism. Soc. Am.* **61**, p. 479.

Watson, G. N. (1966). The theory of Bessel functions, *A Treatise*, University Press, Cambridge.

Lamont-Doherty Geological Observatory
of Columbia University
Palisades, New York 10964
Contribution No. 1724

Manuscript received May 17, 1971